smart cities

MDPI

Article

Mechanism-Driven Intelligent Settlement Prediction for Shield Tunneling Through Areas Without Ground Monitoring

Min Hu [1,2], Pengpeng Zhao [1,3,*], Jing Lu [1,3] and Bingjian Wu [1,2]

[1] SHU-SUCG Research Center for Building Industrialization, Shanghai University, Shanghai 200072, China; minahu@shu.edu.cn (M.H.); lujing98@shu.edu.cn (J.L.); wubingjian0515@163.com (B.W.)
[2] SILC Business School, Shanghai University, Shanghai 201800, China
[3] School of Mechatronic Engineering and Automation, Shanghai University, Shanghai 200444, China
* Correspondence: zhaopengpeng@shu.edu.cn

Highlights:

What are the main findings?

- There is a strong correlation between the resultant force on the shield machine and the center of motion and ground settlement during the propulsion process.
- The mechanism-driven intelligent settlement prediction method (MISPM) can accurately predict settlement ahead of tunnel excavation even without ground monitoring.

What is the implication of the main findings?

- When the shield machine traverses areas where it is difficult to set settlement measurement points, MISPM provides a reliable decision-making basis for optimizing balanced pressure and ensuring environmental safety.
- MISPM can detect changes in ground settlement more quickly than traditional settlement monitoring feedback, improving the efficiency and safety of urban infrastructure construction.

Abstract: Ground settlement is a crucial indicator for assessing the safety of shield tunneling and its impact on the surrounding environment. However, most existing settlement prediction methods are based on historical data, which can only be applied with effective monitoring conditions. To overcome this limitation, this paper proposes the mechanism-driven intelligent settlement prediction method (MISPM), which considers the mechanisms of settlement and attitude movements during construction to design new features that can indirectly reflect settlement. Simulation experiments were used to compare the impact of different candidate features and algorithms on prediction performance, verifying the validity and accuracy of the model. The efficacy of MISPM in predicting settlement changes in advance was substantiated by practical engineering applications. Results showed that MISPM could accurately predict settlement changes even without ground monitoring, thereby corroborating its reliability and applicability in supporting safe tunneling in complex geological environments. In the construction of urban infrastructure, this method has the potential to enhance the efficiency of tunnel construction and ensure environmental safety, which is of great significance for the development of smart cities.

Keywords: shield tunneling; settlement prediction; mechanism-driven; attitude features; XGBoost

Academic Editor: Pierluigi Siano

Received: 18 November 2024
Revised: 17 December 2024
Accepted: 25 December 2024
Published: 27 December 2024

Citation: Hu, M.; Zhao, P.; Lu, J.; Wu, B. Mechanism-Driven Intelligent Settlement Prediction for Shield Tunneling Through Areas Without Ground Monitoring. *Smart Cities* **2025**, *8*, 6. https://doi.org/10.3390/smartcities8010006

1. Introduction

With the acceleration of global economic growth and urbanization, shield tunneling has become a popular technology in urban infrastructure construction. The problem of land subsidence caused by underground space construction is worthy of attention in urban environmental safety. Settlement will affect not only the safety and efficiency of the tunnel construction process but also the stability of nearby buildings and urban facilities [1].

Traditional settlement prediction methods are generally classified into analytical and numerical simulations [2]. Analytical methods employ empirical formulas founded upon foundational parameters and geological conditions to predict maximum ground settlement. Peck put forth a Gaussian formula based on soil loss rate, thereby establishing a ground settlement prediction formula [3]. Zhang et al. [4] created a prediction formula for maximum settlement due to shield excavation using multiple linear regression, considering factors such as shield radius, burial depth, and geological conditions. Jin et al. [5] proposed an empirical formula for the maximum settlement of existing tunnels caused by new tunnel construction based on a mechanical theory regarding the interaction between tunnels and soil. Analytical methods primarily describe settlement distribution curves, offering insight into the maximum ground settlement and its location. However, they are less suited to predicting real-time settlement during shield tunneling.

Numerical simulation methods incorporate construction and geological conditions to model the spatiotemporal characteristics of ground settlement, mainly using finite element and boundary element methods to simulate the changes in settlement induced by shield tunneling. Li et al. [6] used FLAC 3D to establish a three-dimensional model for simulating and predicting ground settlement. Luo et al. [7] established a three-dimensional model through numerical simulation to study the effects of four key factors—thrust, grouting pressure, earth pressure, and formation elastic modulus—on ground settlement in different scenarios. While numerical simulation methods can reflect the settlement process, they often suffer from oversimplified models and difficulty in determining internal parameters, which limits their accuracy and typically restricts their use to examining the relationship between construction parameters and settlement effects.

Although models incorporating numerical parameter inversion [8] achieve significantly higher prediction accuracy by adjusting model parameters with actual data, such methods require extensive time for parameter optimization and offer limited generalizability, making them challenging to apply in practical engineering contexts.

In recent years, machine learning has seen significant advances in applications for tunnel settlement prediction [9,10]. Hu et al. [11] analyzed various stages of settlement development and used a BP neural network to model and predict the final settlement. Zhou et al. [12] employed the XGBoost algorithm to predict maximum settlement based on tunnel depth, overburden thickness, and grouting volume. Zhang et al. [13] used settlement monitoring data to develop a prediction model based on LSTM, utilizing the previous ten time-sequential data points to predict the current ground settlement. Similarly, Ning et al. [14] designed an LSTM-based settlement prediction model that uses the last six data points from relevant monitoring locations to predict settlement at a target point based on time-series ground settlement data. Machine learning techniques can achieve relatively accurate real-time settlement predictions compared to traditional methods. However, these methods typically require continuous model updates and recalculations based on the latest monitoring data, often leading to overfitting and weak generalization. If geological conditions or other operational factors change, the model's accuracy may decline significantly [15], limiting its application in different projects.

However, the frequency of settlement monitoring is low, and the data are sometimes difficult to obtain. In practical engineering contexts, data are only recorded once every 12 h

due to monitoring cost constraints. Settlement monitoring is difficult when crossing rivers, airports, or other special areas. In these areas, ground settlement monitoring intervals may be longer, or data may not be available at all, making them weak monitoring scenarios. Although settlement monitoring is difficult in weak monitoring scenarios, this does not mean that settlement monitoring is unnecessary. For example, strict control of ground deformation is essential in airport areas, as excessive settlement could result in runway unevenness, leading to accidents. When tunneling under rivers, settlement control seems less critical. However, if ground settlement occurs, it will lead to tunnel flooding and serious accidents. It is crucial to identify a settlement prediction method that is not overly reliant on real-time monitoring data to enhance the practical utility of such models. This method can accurately predict settlement trends in real time under weak monitoring conditions, assist in construction project decision-making, and better ensure the efficiency and safety of sustainable urban infrastructure construction.

In the absence of settlement monitoring data, accurate prediction of settlement requires identification of features that can capture ground settlement (or soil deformation). As the shield machine advances, it alters the pressure distribution in the soil ahead of the excavation face, leading to soil subsidence or heave. Simultaneously, the machine leaves voids behind it, and if these voids are not promptly, adequately, or properly grouted, additional ground loss can occur. According to Newton's Third Law of Motion, for every action force, there is an equal and opposite reaction force. Thus, the deformation force in the soil surrounding the shield also acts on the shield machine, causing its movement behavior to differ from normal conditions. Based on this premise, this study seeks to explore the relationship between the shield machine's mechanical load and attitude motion trends and ground settlement. It aims to construct features that can reflect settlement without relying on monitoring data, thereby developing a real-time settlement prediction method suitable for weak monitoring scenarios and improving the efficiency and safety of urban infrastructure construction.

This paper focuses on the ground settlement ahead of the shield tunnel excavation face, discussing how efficient and accurate prediction can be achieved under weak monitoring conditions. This paper is organized into six sections. The remainder of the structure is as follows: Section 2 introduces the settlement ahead of the excavation face and the forces acting on the shield machine, analyzing force variations and movement dynamics. Section 3 provides a detailed analysis of the factors influencing settlement, describing the design process of the prediction framework and model. Section 4 presents experimental case studies, analyzing prediction results and the importance of features to validate the proposed method's rationality, accuracy, and applicability. Section 5 applies this method to practical engineering, assisting on-site decision-making and providing timely recommendations for construction parameter adjustments. Section 6 concludes this paper and offers perspectives for future work.

2. Ground Settlement and Shield Force State

During shield tunneling construction, the soil ahead of the shield machine is subjected to surrounding stress and surface loading, leading to ground deformation and potentially causing ground settlement or heave. Depending on the geological loss, the soil's bearing capacity and deformation characteristics will vary, affecting the degree of soil disturbance [16]. The force situation of shield tunneling is shown in Figure 1.

The force F exerted by the shield machine on the surrounding soil ahead of the excavation face is met with a reactive soil pressure acting on the shield machine itself. As settlement occurs, the soil structure changes, resulting in a redistribution of the earth pressure ahead of the excavation face, which in turn affects the stability of the excavation

face [17,18]. Concurrently, these changes in loading also alter the shield machine's original attitude and motion.

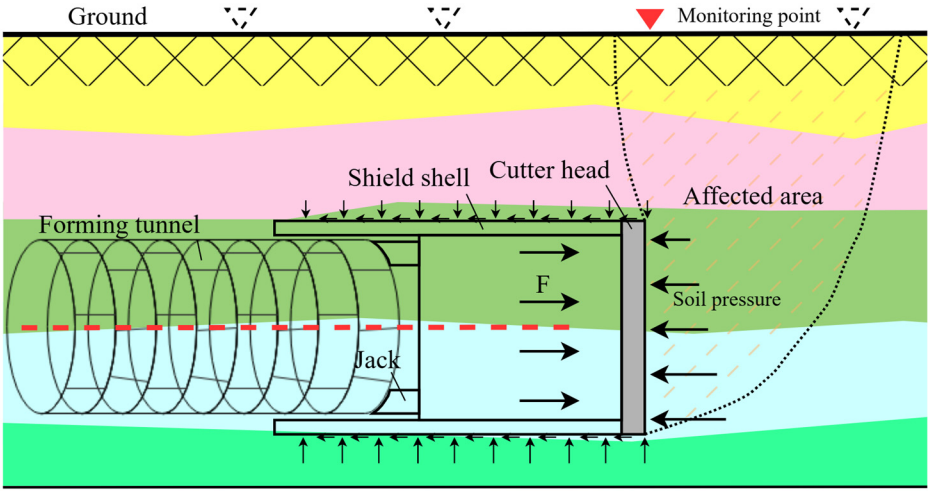

Figure 1. Shield machine force state during tunneling.

When excessive settlement occurs in front of the shield machine, the earth pressure ahead of the excavation face shifts, causing unsupported soil to move toward the tunnel, further increasing the earth pressure on the front of the shield. In weak strata or areas with high groundwater levels, soil cohesion is relatively low. Once the soil structure is compromised, it may become loose, potentially changing the soil pressure ahead of the excavation face [19].

Ground settlement destabilizes the forward pressure, leading to fluctuating, difficult-to-control earth pressure levels. These pressure variations alter the shield machine's loading conditions, impacting its attitude and motion patterns [20]. Therefore, by analyzing the relationship between the shield machine's loading, changes in its attitude and motion, and the earth pressure at the excavation face, it may be possible to detect changes in the soil distribution ahead of the excavation face, infer its stability, and thereby accurately predict variations in ground settlement.

2.1. Force Analysis of the Shield Machine

During the tunneling process, the shield machine can be simplified as a rigid cylindrical body with a slope angle β. Figure 2 details the forces acting on the shield machine.

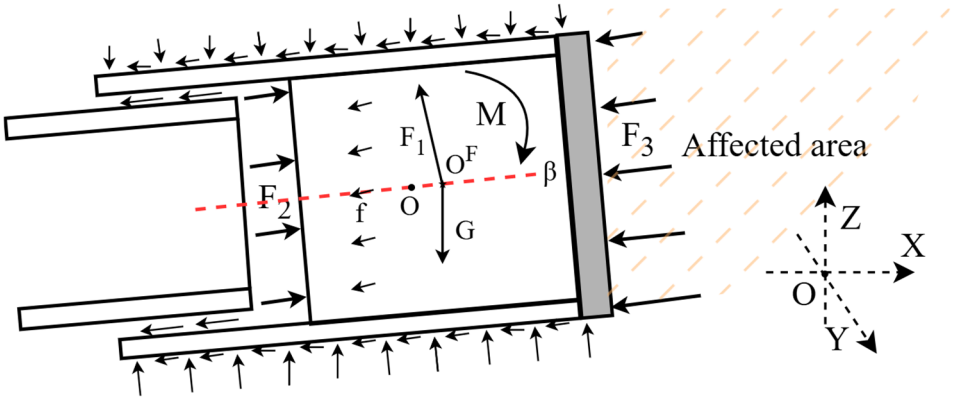

Figure 2. Mechanical analysis of the shield machine.

In the figure, the shield propulsion direction is along the X-axis, the horizontal direction is Y, and the vertical direction is Z. The weight of the shield m is such that it is always

subjected to a vertically downward gravitational force G. The vertical support force F_1 balances both the machine's weight and the soil load above it. The thrust F_2 represents the reaction force exerted by the hydraulic jacks on the segmental lining, pushing the shield forward. Friction f occurs between the surrounding soil and the machine, acting opposite to the direction of movement. Additionally, the forward soil exerts a reaction force F_3 on the cutting face, which is calculated from the sensor values.

These forces collectively act on the shield machine, forming a resultant force at a center point O^F. If this center does not coincide with the center of mass O, the machine will experience both translational motion [20] and rotational motion. In this situation, an "eccentricity distance" arises between the two points, generating a resultant moment M that induces rotation in the shield machine. The equations governing the force and moment analysis of the shield machine are shown in Equation (1):

$$\begin{cases} F = ma \\ M = d \times F = I * \alpha \\ O_x^F = L/2 - d \end{cases} \tag{1}$$

Here, the linear acceleration a, moment of inertia I, and angular acceleration α are solved based on the shield machine's cutting face and real-time position changes. F represents the force on one side of the moment, and d is the eccentricity between the resultant force point and the center of mass. The length of the shield machine is L, and the distance from the resultant force point to the cutting face is denoted as O_x^F. Changes in the forces and moments at the resultant force point will affect the machine's mechanical properties and its attitude motion. By analyzing the position of the resultant force point, the mechanical state of the shield machine can be reflected, which in turn provides an indication of ground settlement variations to some extent.

2.2. Motion Analysis of the Shield Machine

When the forces exerted by the surrounding soil on the shield machine change, the resultant force and moment will also change, affecting the shield's motion pattern. The magnitude of the resultant force is primarily determined by the shield machine's advancement speed, which is mainly influenced by the machine's attitude before and after propulsion. The attitude variation during propulsion is shown in Figure 3.

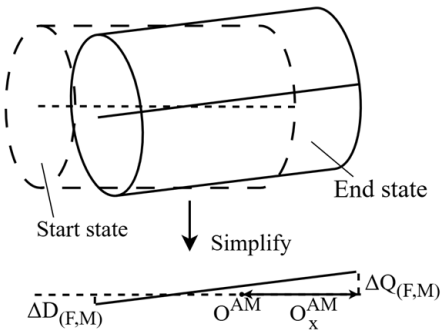

Figure 3. Status of attitude changes during advancement.

Based on the force analysis in Section 2.1, the motion center point of a ring can be calculated as shown in Equation (2):

$$O_x^{AM} = \frac{\left(\left|\Delta Q_{(F,M)}\right| + 2\left|\Delta D_{(F,M)}\right|\right)L}{3\left(\left|\Delta Q_{(F,M)}\right| + \left|\Delta D_{(F,M)}\right|\right)} \tag{2}$$

In the equation, O_x^{AM} represents the distance from the motion center point O^{AM} to the cutting face. $\Delta Q_{(F,M)}$ is the elevation change at the cutting face before and after propulsion, calculated using the change in attitude, $\Delta Q_{(F,M)} = Qz_{end} - Qz_{start}$. Similarly, $\Delta D_{(F,M)}$ represents the elevation change at the tail of the shield machine before and after propulsion, with the calculation method being similar to the former. According to the actual attitude and position of the shield machine, the resultant force point and motion center point of the shield machine can be calculated [21].

3. Settlement Prediction Model

3.1. Selection of Influencing Factors

Figure 4 counts the influence factors mentioned in the papers related to subsidence prediction in the Web of Science database in the last five years. These can be classified into geometric parameters, geological conditions, tunneling factors, and tail grouting [12,15,22–29].

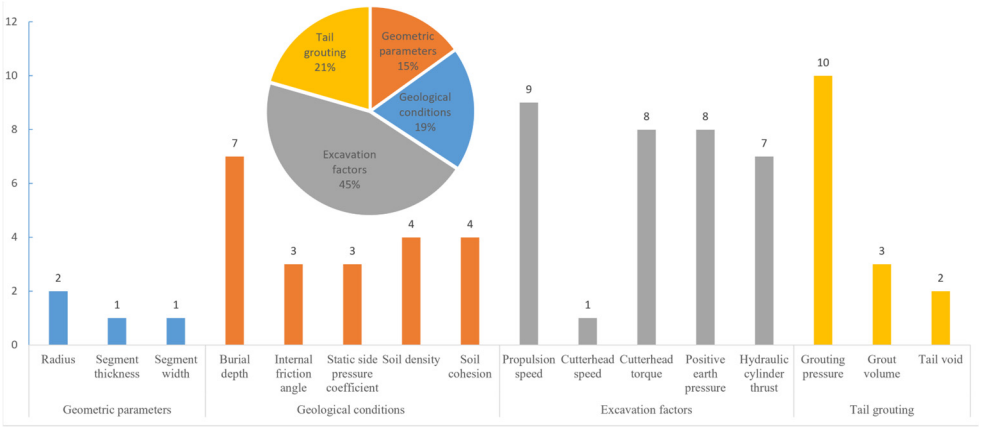

Figure 4. Impact factors considered in relevant studies.

The geometric parameters include tunnel radius, segment thickness, and segment width, but these factors are used less frequently. The relevant parameters of the segments are excluded, as they mainly affect the final settlement, and their impact on the settlement ahead of the tunnel face can be neglected. Geological conditions are mentioned more often. The depth of burial is mentioned six times. Factors such as the angle of internal friction and the coefficient of static lateral pressure are also frequently mentioned. This indicates that geological conditions have a major influence on ground settlement, particularly the depth of burial, which directly affects the distribution of stresses in the strata and the stability of the soil layer.

Most studies suggest that tunneling factors such as propulsion speed and cutter head torque significantly influence ground settlement in the tunneling process, indicating a strong relationship between tunneling factors and ground settlement. The tunneling parameters affect the ground settlement, especially in the process of controlling ground settlement, and the adjustment of tunnel parameters is crucial. Tail grouting has received significant attention in predicting final settlement, as grouting pressure directly affects the filling of voids and the reinforcement of the strata, influencing soil deformation and final settlement. However, this study focuses on predicting the settlement ahead of the tunnel face, where the impact of tail grouting on settlement at monitoring points ahead of the tunnel face is negligible. Based on the analysis of the above factors, the relevant parameters of segments and tail grouting are excluded, and geometric parameters, geological conditions, and tunneling factors are considered.

According to geological conditions and Coulomb's earth pressure theory [18], the upper soil layer's load is considered as an overload on the lower soil layer, which leads to

dividing the load into upper and lower parts of the shield machine to account for different geological situations. Additionally, combining the analysis in Section 2, the length and weight of the shield machine are considered, introducing attitude factors and the positions of the resultant force point and motion center as input variables for the prediction model. The candidate features are shown in Table 1.

Table 1. The candidate feature set of the model.

Feature Group	Feature Parameters	Symbol	Unit	Data Sources
Geometric parameters (GP)	Radius	r	mm	TBM report
	Shield length	L	mm	
Geological conditions (GC)	Burial depth	Depth	m	Geological exploration
	Internal friction angle	φ	deg	
	Static side pressure coefficient	K_0	-	
	Soil density	γ	kN/m^3	
	Soil cohesion	c	Pa	
	Upper load	σ_v^{up}	bar	Theoretical analysis
	Lower load	σ_v^{down}	bar	
Excavation factors (EF)	Propulsion speed	Ps	mm/min	Sensor measurement
	Cutterhead speed	Cs	rpm	
	Cutterhead torque	Ct	kN×m	
	Positive earth pressure	F_3	kN	
	Hydraulic cylinder thrust	F_2	kN	
	Shield gravity	G	kN	TBM report
Attitude features (AF)	Slope angle	β	deg	Sensor measurement
	Elevation deviation of incision	Qz	mm	
	Elevation deviation of tail	Dz	mm	
Motion features (MF)	Location of the joint force point	O_x^F	mm	Theoretical analysis
	Location of the motion center point	O_x^{AM}	mm	

The variation in ground settlement affects the forces acting on the shield machine, causing the position of the resultant force point to change. Mechanical relationship analysis takes into account the geometric parameters, weight, and slope angle of the shield machine, establishing force and moment equations to determine the position of the resultant force point. Changes in these mechanical relationships also influence the overall equilibrium of the shield machine, altering its attitude motion trend. By analyzing the elevation deviations at the cutting face and the tail of the shield before and after advancement, the machine's attitude motion can be assessed, leading to the identification of the motion center. Through the analysis of settlement mechanisms, mechanical relationships, and attitude motion, the attitude and motion characteristics can indirectly reflect changes in ground settlement.

3.2. Settlement Prediction Model Construction

Based on the settlement mechanism and the analysis of force and attitude motion, this paper proposes the mechanism-driven intelligent settlement prediction method (MISPM). The overall framework for ground settlement prediction includes five modules—data preprocessing, feature reconstruction, data enhancement, model training, and prediction output—as shown in Figure 5.

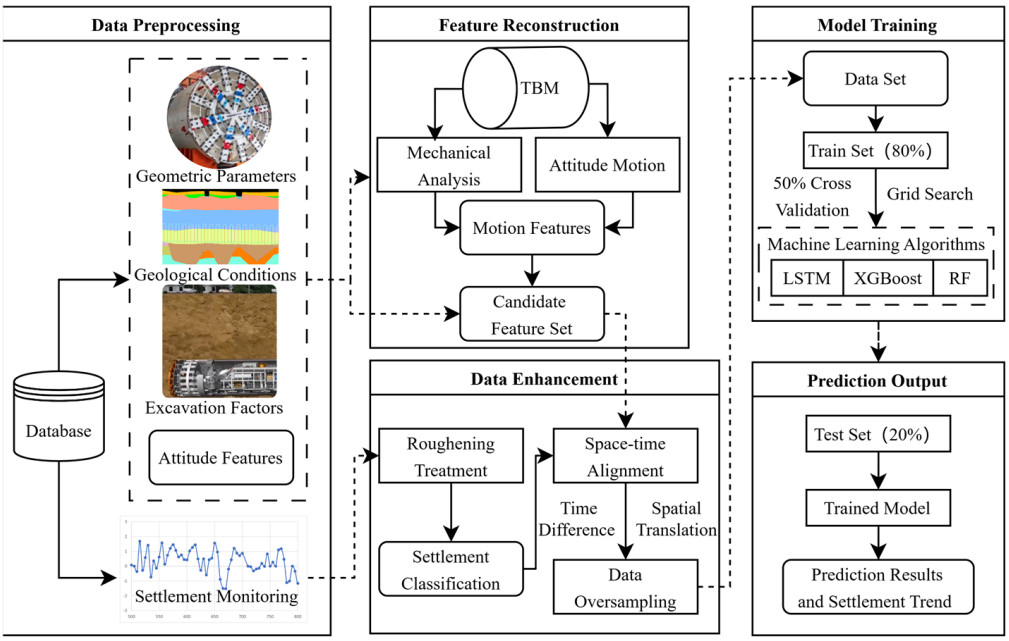

Figure 5. Mechanism-driven intelligent settlement prediction method.

The data preprocessing module processes the geometric parameters, geological conditions, tunneling factors, attitude characteristics, and settlement monitoring data. As missing and anomalous data may occur, interpolation is applied to fill in small amounts of missing data. At the same time, outliers are removed using the Z-score method with a specified threshold.

The feature reconstruction module calculates the shield machine's resultant force point and motion center, combined with other factors affecting settlement, to form a candidate feature set.

In the data augmentation module, ground settlement data undergoes roughening to derive corresponding settlement classifications. Additionally, data from different sources are aligned across time and space dimensions using spatiotemporal alignment and oversampling methods for data enhancement.

In the model training module, the processed data is split into training and test sets at a four-to-one ratio. During training with various machine learning algorithms (e.g., LSTM, XGBoost, and RF), five-fold cross-validation and grid search techniques are employed to identify the optimal model parameters. The prediction output module applies the trained model to the test set to predict ground settlement and trend changes, outputting the predicted results and settlement trends.

These five modules form the ground settlement prediction framework, where feature reconstruction and data augmentation enhance model prediction performance and provide reliable predictions and settlement trends to ensure construction safety and quality control.

3.3. Data Preparation

3.3.1. Discretization of Settlement Data

The goal of ground settlement prediction is to identify potentially significant surface uplift and settlement trends early, enabling timely response measures to ensure project safety. For settlement prediction, the focus lies on accurately predicting settlement quantities and grasping settlement trend changes. Therefore, this study discretizes settlement values based on safety characteristics.

Drawing on the Chinese national standards (GB 50911-2013) [30], the daily change amount of deformation should be limited to less than 3 mm. In practical engineering

applications, stricter thresholds are executed. Generally, the alert threshold for deformation changes between adjacent measurements (12 h interval) is set at ±0.5 mm. Therefore, in this paper, settlement grades are based on the amount of change in 12 h soil settlement, and the specific rules are shown in Table 2.

Table 2. Ground deformation grade.

Grade	High Subsidence	Subsidence	Stable	Heave	High Heave
Label	0	1	2	3	4
Ground deformation change (mm)	$(-\infty, -1.5]$	$(-1.5, -0.5]$	$(-0.5, 0.5)$	$[0.5, 1.5)$	$[1.5, \infty)$

By categorizing ground deformation data based on the change in 12 h intervals, five grades are defined—high subsidence, subsidence, stable, heave, and high heave—with a classification label assigned to each. The goal is to convert continuous variables into discrete categories, making it easier for the model to capture settlement trends and patterns.

3.3.2. Space–Time Alignment

To ensure the effective use of construction and settlement monitoring data, it is critical to align them in both time and space. This alignment bridges the gap between different data collection frequencies and spatial references, enabling accurate prediction of settlement behavior. Temporal alignment ensures that settlement and tunneling parameters are synchronized over time, while spatial alignment adjusts for the positional relationship between the shield machine and its impact zone.

1. Temporal alignment

The construction and settlement data must be synchronized to ensure data consistency, although the data have different sampling frequencies. The settlement frequency is typically low, often once or twice daily, whereas shield tunneling data is very high, with one record per second.

To address this discrepancy, tunneling parameters are aggregated by "ring", calculating their average values per ring. Then, settlement monitoring times are used to track corresponding advance rings. For two adjacent monitoring times, specifically the previous monitoring time t_p and the current time t, the corresponding ring numbers are $N(t_p)$ and $N(t)$.

If $N(t_p) \neq N(t)$, this indicates that the ring number changed within the monitoring time gap, with the shield machine having advanced by $N(t) - N(t_p)$ rings. After that, based on the time taken for each ring advance, the previous monitoring value is used as a reference, interpolating to estimate the settlement change in front of the cutting face. If $N(t_p) = N(t)$, it indicates that no advance occurred during this period. In this case, the average of the two monitoring data points is taken as the settlement change in front of the cutting face. This method effectively aligns construction and settlement monitoring data over time, providing data support for subsequent settlement prediction.

2. Spatial alignment

The ring number remains the fundamental unit for spatial calibration. However, the ring number represents the position of the tail of the shield, whereas the forward settlement is influenced by the cutting of the head of the shield. Consequently, for the acquisition of geological data and geometric parameters, a forward movement of one shield length is necessary, and the settlement data must be shifted to align with the data within the influence of the shield tail in front.

If the shield length is 10 m and the width of each ring is 2 m, the length of five rings is obtained. The settlement influence area is 8 m, which is the length of four rings.

Consequently, when the ring number for shield tunneling is N, the corresponding geological data and geometric parameter data are derived from the data of the N + 5 ring, while the data about the settlement are sourced from N + 5 to N + 9. The shield tunneling parameters do not need to be spatially shifted, as shown in Figure 6.

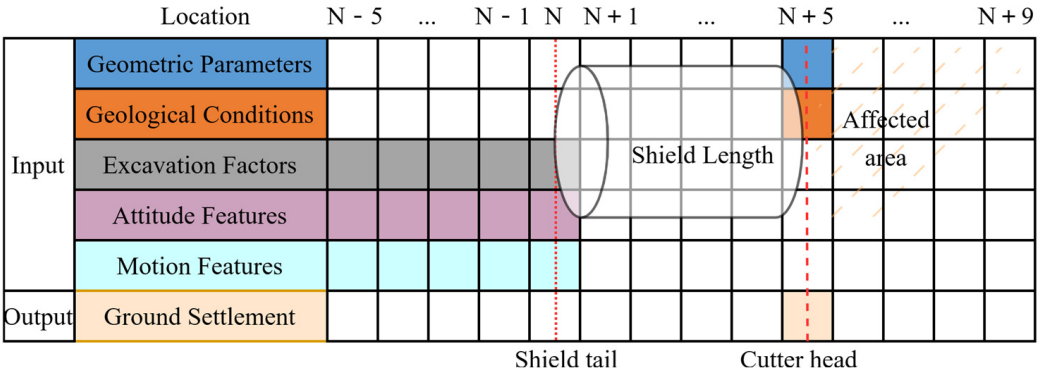

Figure 6. Spatial alignment of data.

During tunnel construction, multiple monitoring points are deployed. To represent settlement, the mean value of the settlement is calculated across several monitoring points situated within the zone of influence in advance of the cutting face. This approach ensures the monitoring of ground settlement is conducted with accuracy.

3.3.3. Oversampling

Ground settlement data often suffers from significant class imbalance, with fewer samples in categories experiencing high subsidence or heave. Random oversampling [31,32] is employed to balance the dataset by duplicating existing samples from minority classes. This approach ensures a more equitable distribution across classes, enabling the model to learn from minority class samples more effectively and reducing its bias towards the majority class.

By conducting settlement data discretization, performing spatiotemporal alignment, and implementing oversampling, the settlement categories are balanced, and discrepancies across data sources are resolved. This process ensures the accuracy and consistency of the dataset, providing the model with a robust and reliable foundation upon which to enhance prediction performance and model robustness.

3.4. Prediction Algorithm Selection

The relationship between ground settlement and influencing factors is complex and nonlinear, making linear models insufficient for accurate prediction. Machine learning algorithms excel at handling nonlinearity, enhancing prediction accuracy and reliability. Table 3 presents a partial overview of the application of common machine learning algorithms in ground settlement research over recent years.

Table 3. Application of different algorithms.

Algorithm	Related Research
RF	Hu et al. [24], Yang et al. [26], Ling et al. [27], Zhou et al. [28], Cheng et al. [29], and Wu et al. [33]
XGBoost	Zhou et al. [12], Su et al. [15], Zhang et al. [25], Gu et al. [34], and Bo et al. [35]
LSTM	Zhang et al. [13], Ning et al. [14], Zhang et al. [36], Ye et al. [37], and He et al. [38]
SVR	Bai et al. [10] and Pan et al. [31]
SVM	Cheng et al. [32]
BP	Hu et al. [11]
ANN	Chen et al. [9]

According to Table 3, random forest (RF) has the highest frequency of occurrence, followed by extreme gradient boosting (XGBoost) and long short-term memory (LSTM). Therefore, this study chose LSTM, XGBoost, and RF as candidate prediction algorithms.

4. Simulation Experiment

4.1. Experimental Design

The experiment data were sourced from rings 500 to 1200 of the Right Line in Shanghai's section 12 project to verify the reasonableness and accuracy of the settlement prediction method. The experiment had three objectives: comparing the predictive performance of the base algorithms LSTM, XGBoost, and RF; analyzing the impact of features on the performance of the settlement prediction model; and determining the optimal structure of the settlement model.

The Shanghai Airport Line's section 12 Lingfeng interval Right Line tunnel project encompasses a total length of 5695 m and comprises 3164 rings. The construction of this tunnel was completed using an earth pressure balance (EPB) shield machine. The shield machine has a length of 11.44 m, a radius of 4.65 m, and a mass of approximately 800 tons. The tunnel segments were 450 mm in thickness, with a ring width of 1.8 m. As illustrated in Figure 7, the shield machine advanced through a clay layer comprising gray muddy clay and gray clay.

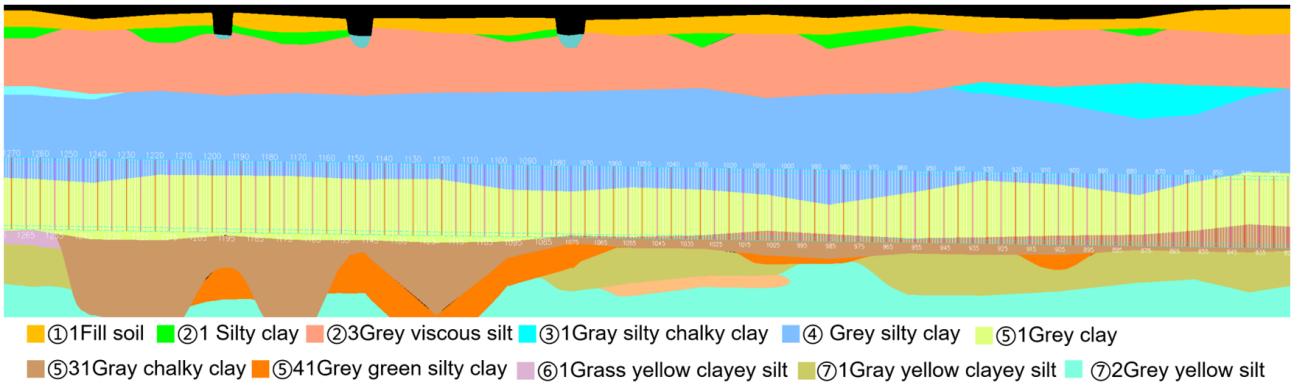

Figure 7. Geological profile of Shanghai section 12 Right Line.

Following the application of the methodology delineated in Section 3.3, a total of 290 records were yielded. Subsequently, the processed dataset was divided into a training set and a test set in a 4:1 ratio, thereby facilitating the construction of the settlement prediction model. Once the model had been trained, it was employed to predict ground settlement on the test set, thus facilitating model evaluation and optimization.

4.1.1. Model Design

Settlement prediction models were constructed using various machine learning methods. To address class imbalance, the LSTM model employed a categorical cross-entropy loss function, while the XGBoost and RF models used oversampling to balance settlement classes.

Model training incorporated 5-fold cross-validation to maximize data utilization and reduce overfitting risk. Grid search was applied for hyperparameter optimization to determine optimal parameter configurations, as shown in Table 4.

Table 4. Model parameters for different algorithms.

Algorithm	Parameters
LSTM	'epochs': 10, 'batch_size': 10, 'dropout_rate': 0.5, 'neurons': 32, 'optimizer': 'adam', 'activation': 'softmax', 'loss ': 'categorical_crossentropy ',
XGBoost	'colsample_bytree': 0.8, 'learning_rate': 0.3, 'max_depth': 3, 'n_estimators': 50, 'subsample': 0.6, 'gamma': 0.2
RF	'max_depth': 10, 'min_samples_leaf': 2, 'min_samples_split': 5, 'n_estimators': 50

The experiment employed Python libraries, including XGBoost (1.7.6), scikit-learn (1.2.2), and TensorFlow (2.12.0), to implement the settlement prediction models. It compared the performance of three algorithms, namely LSTM, XGBoost, and RF, and also analyzed the impact of different selected features on model performance. The comparative analysis was conducted from two perspectives: the choice of algorithm and the selection of input features. Detailed descriptions of each experimental condition are provided in Table 5.

Table 5. Experiment list.

No	Name	Predict Algorithm	Select Features
1	LSTM_BF	LSTM	GP, GC, and EF
2	LSTM_AF	LSTM	GP, GC, EF, and AF
3	LSTM_MF	LSTM	GP, GC, EF, and MF
4	LSTM_PMD	LSTM	GP, GC, EF, and MF + PMD
5	XGboost_BF	XGboost	GP, GC, and EF
6	XGboost_AF	XGboost	GP, GC, EF, and AF
7	XGboost_MF	XGboost	GP, GC, EF, and MF
8	XGboost_FR	XGboost	GP, GC, EF, and MF + FR
9	RF_BF	RF	GP, GC, and EF
10	RF_AF	RF	GP, GC, EF, and AF
11	RF_MF	RF	GP, GC, EF, and MF
12	RF_FR	RF	GP, GC, EF, and MF + FR

The candidate feature set included GP, GC, EF, AF, and MF. Relevant features were selected from these. The first three types of features were basic. Attitude and motion features were introduced later. The radius, length, and gravity of the shield machine were constant, so they were not included in the model.

Due to the consideration of previous monitoring data (PMD) in most settlement studies of LSTM, LSTM_PMD used the data to predict ground settlement. Feature reduction (FR) was employed to identify the six most salient features, as determined by their ranking of importance in the XGBoost and RF algorithms.

4.1.2. Model Evaluation

As settlement prediction is a multi-class problem, this study employed the micro-average method [39] to evaluate the model's prediction results and performance. The model treated its class as the positive class and the others as the negative class. The metrics for each class were calculated based on the corresponding true positives (TP_i), false positives (FP_i), false negatives (FN_i), and true negatives (TN_i), from which the precision, recall, F1 score, and accuracy of the classification model were computed, as shown in Equation (3), where n represents the total number of classes, which is equal to five, and Num^{total} is the total number of samples.

$$\begin{cases} Precision = \frac{\sum_{i=1}^{n} TP_i}{\sum_{j=1}^{n} TP_j + FP_j} \\ Recall = \frac{\sum_{i=1}^{n} TP_i}{\sum_{j=1}^{n} TP_j + FN_j} \\ F1 = 2 \times \frac{Precision \times Recall}{Precision + Recall} \\ Accuracy = \frac{\sum_{i=1}^{n} TP_i}{Num^{total}} \end{cases} \quad (3)$$

4.2. Results and Analysis

4.2.1. LSTM Algorithm

The prediction performance of the LSTM algorithm-based prediction model using different input features is shown in Table 6.

Table 6. Prediction performance of LSTM under different features.

	Train				Test			
	Precision	**Recall**	**F1**	**Accuracy**	**Precision**	**Recall**	**F1**	**Accuracy**
LSTM_BF	0.21	0.45	0.28	0.45	0.10	0.32	0.16	0.32
LSTM_AF	0.21	0.45	0.28	0.45	0.10	0.32	0.16	0.32
LSTM_MF	0.10	0.31	0.15	0.31	0.15	0.39	0.22	0.39
LSTM_PMD	0.65	0.68	0.63	0.68	0.66	0.70	0.65	0.70

LSTM_BF exhibited poor performance in both the training and testing sets, with an accuracy of 0.32 and an F1 score of 0.16. Similarly, LSTM_AF, which incorporated attitude features, showed no significant improvement, indicating that the addition of attitude features alone did not substantially enhance predictive capability. However, integrating motion features (LSTM_MF) resulted in a modest improvement, with test set accuracy increasing to 0.39, though the overall performance was still poor.

A comparison between LSTM_MF and LSTM_PMD demonstrated a notable improvement in prediction accuracy, rising from 0.39 to 0.70. The confusion matrices for the model under these conditions are presented in Figure 8.

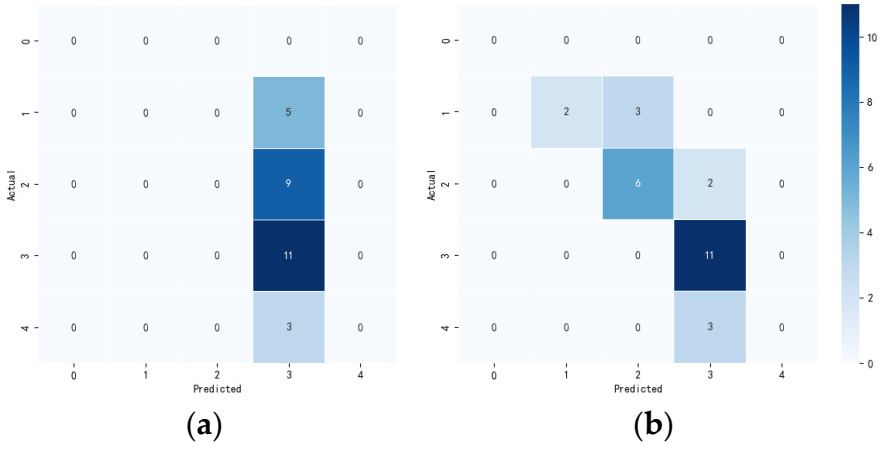

Figure 8. Confusion matrix of LSTM under different conditions. (**a**) LSTM_MF; (**b**) LSTM_PMD.

The confusion matrix displays the differences between the predicted results of different categories and the actual classification, with rows representing the predicted settlement categories and columns denoting the actual categories. As can be seen, LSTM_MF tended to classify most cases as having no significant subsidence changes, failing to accurately identify surface subsidence and heave. In contrast, LSTM_PMD partially overcame these limitations, demonstrating improved predictive performance.

Accordingly, the LSTM algorithm was contingent upon the availability of previous monitoring data. In the absence of such data, the predictive outcomes tended to be over-simplified, thereby impeding the capacity to accurately predict ground settlement.

4.2.2. XGBoost and RF Algorithm

According to the experimental design, a settlement prediction model was established using XGBoost and RF algorithms, and the predictive performance of the model under different features was compared and evaluated, as shown in Table 7.

Table 7. Prediction performance of XGBoost and RF under different features.

	Train				**Test**			
	Precision	**Recall**	**F1**	**Accuracy**	**Precision**	**Recall**	**F1**	**Accuracy**
XGboost_BF	1.00	1.00	1.00	1.00	0.72	0.76	0.74	0.76
XGboost_AF	1.00	1.00	1.00	1.00	0.77	0.79	0.78	0.79
XGboost_MF	1.00	1.00	1.00	1.00	0.80	0.81	0.80	0.81
RF_BF	0.99	0.99	0.99	0.99	0.75	0.74	0.74	0.74
RF_AF	1.00	1.00	1.00	1.00	0.82	0.83	0.82	0.83
RF_MF	1.00	1.00	1.00	1.00	0.84	0.84	0.83	0.84

XGboost_BF performed well on the training set and decreased somewhat on the test set, with an accuracy of 0.76 and an F1 score of 0.74. The prediction performance of XGBoost_AF improved, and the attitude features contributed to the settling prediction. With the introduction of motion features (XGBoost_MF), the metrics of the test set eventually improved by about 0.08, and these features significantly improved the generalization ability and prediction accuracy of the model.

The prediction performance of RF_BF was similar to that of XGboost_BF, with an accuracy of 0.74 and an F1 score of 0.74. After the addition of the attitude features, the prediction performance of RF_AF was significantly improved in the test set, indicating that the attitude features had a greater enhancement on the prediction performance. The accuracy and recall of RF_MF in the test set reached 0.84, and the motion feature's prediction performance of the settlement enhancement was a little better.

According to the confusion matrix between the prediction results and the actual categories, the performance of XGBoost and RF on different settlement categories was evaluated by comparing the settlement prediction performance under the three feature combinations, as shown in Figure 9.

Using XGBoost_BF, it was difficult to accurately distinguish between stable and heave cases, and the model was prone to misclassification problems. By introducing gesture features, the performance of the model improved, and the error of the model prediction was reduced. Although a small number of samples were still misclassified, the error categories were closer to the actual categories, and the prediction ability of XGBoost_MF on slight rumble improved.

With random forest (RF), the model also suffered from the problem of recognition difficulties, misclassifying other categories as steady states. The performance of RF_AF improved, and the cases of non-identification were reduced, but the model still suffered from errors in distinguishing neighboring categories. The prediction performance of RF_MF was enhanced, especially in identifying subsidence and uplift, which reduced the confusion between neighboring categories and improved the accuracy and robustness of the model.

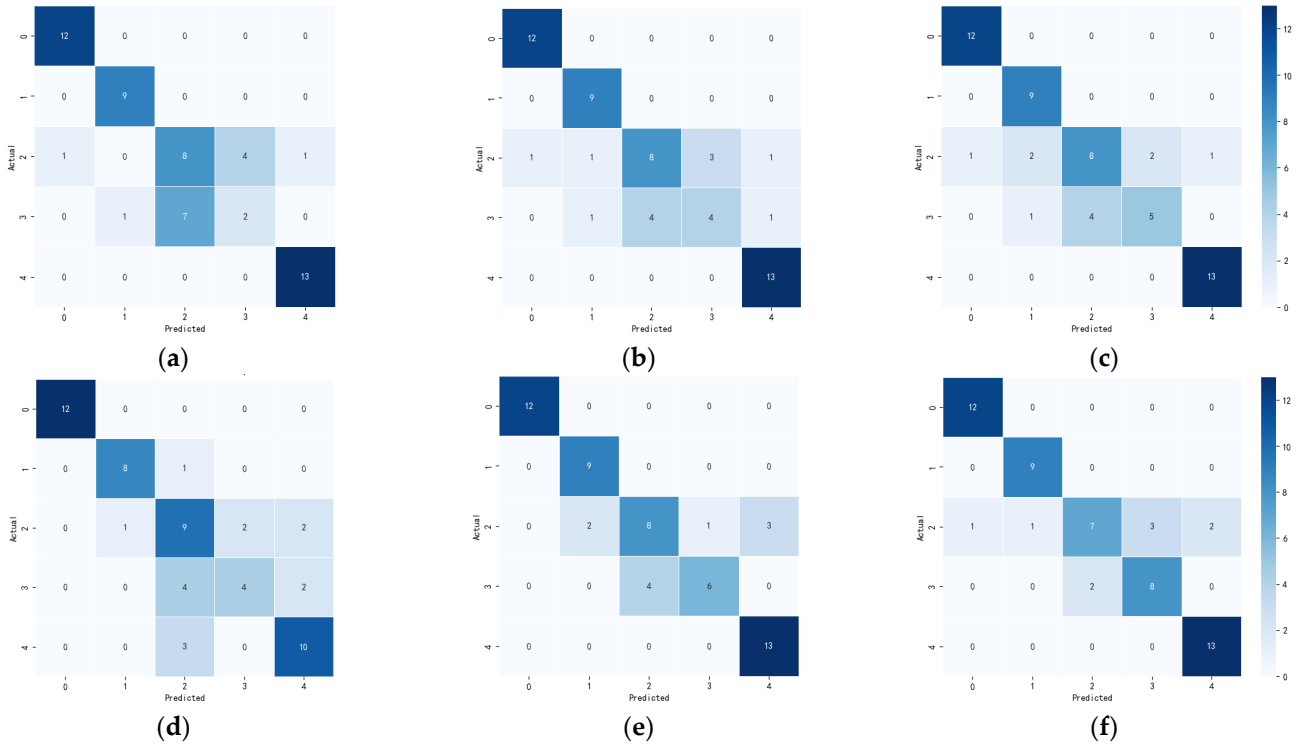

Figure 9. Confusion matrix of XGBoost and RF under different conditions. (**a**) XGboost_BF; (**b**) XGboost_AF; (**c**) XGboost_MF; (**d**) RF_BF; (**e**). RF_AF; (**f**) RF_MF.

With the introduction of attitude or motion features, the model could better distinguish different subsidence categories, narrowing the gap between model prediction and actual classification. The combination of mechanical relations and attitude motion law not only improved the prediction performance of the model, which could better predict the settlement changes and trends, but also enhanced the differentiation and identification ability of the model. The settlement prediction showed it was more accurate and detailed, with good accuracy and reliability.

4.2.3. Features Importance Analysis

From the above experiments, it can be seen that the prediction performance of the model of LSTM, either by introducing attitude or motion features or considering the previous settlement monitoring data, was poor and unsuitable for solving the ground settlement classification problem in this study. The models built by XGBoost and random forest (RF) algorithms achieved good results.

In particular, the introduction of attitude and motion features significantly improved the ability of the models to predict settlement. The order of importance of the input features in the different models is shown in Figure 10.

As can be seen, depth, Ps, Cs, Ct, F_3, and F_2 have high importance in XGBoost_BF and RF_BF. After adding pose features, β and Dz in XGBoost_AF rank among the top six in feature importance, while Qz in RF_AF ranks among the top six in feature importance. With the introduction of motion characteristics, σ_v^{up}, O_x^F, and O_x^{AM} become the top three features of the two algorithms. σ_v^{up} can replace burial depth and geological parameters, and the O_x^F and O_x^{AM} obtained by considering mechanical and attitude motion have an important impact on the prediction of settlement.

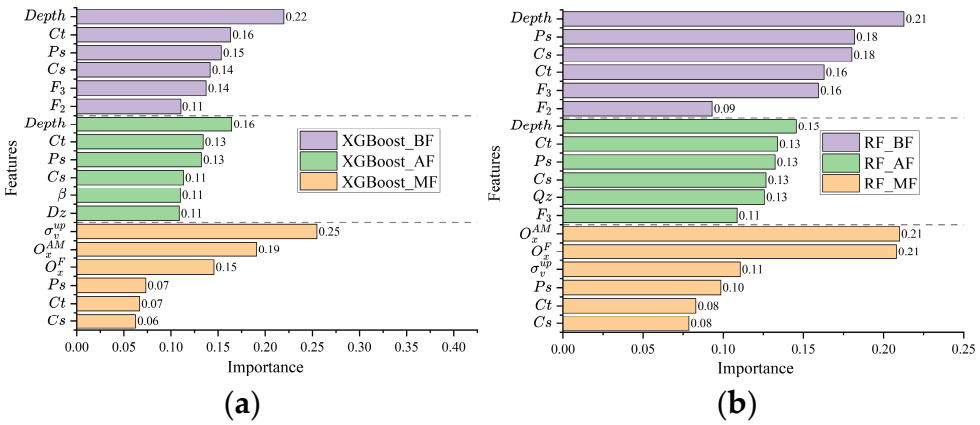

Figure 10. Analysis of the importance of XGBoost and RF features. (**a**) XGBoost; (**b**) RF.

According to the ranking of feature importance, the first six features of XGBoost_MF and RF_MF are consistent. The six features, namely σ_v^{up}, O_x^F, O_x^{AM}, Ps, Cs, and Ct, were therefore selected as model inputs for feature reduction. The performance of the model in surface subsidence prediction before and after feature reduction is shown in Figure 11.

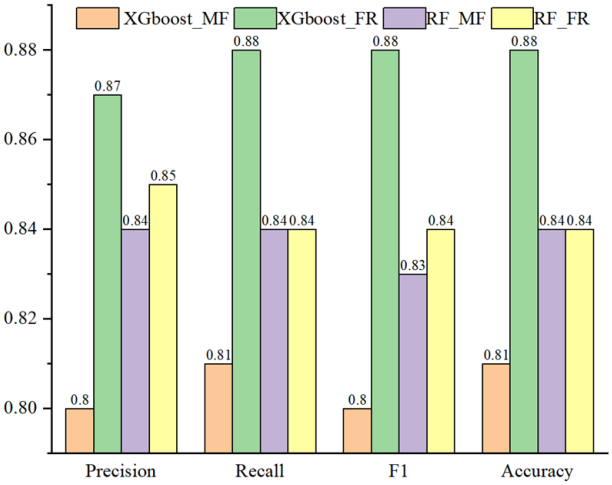

Figure 11. Prediction performance of XGBoost and RF models.

Following the simplification of the features, it is evident that the predictive performance of XGBoost significantly improved, with various indicators improving by about 0.07 and accuracy increasing to 0.88. The predictive performance of RF was relatively stable, with an improvement of 0.01 in precision and F1, without significant change in the indicators before and after. A comparative analysis of algorithms revealed that XGBoost exhibited superior prediction performance in comparison to RF. Furthermore, the incorporation of FR to eliminate redundant features in the model, in contrast to MF, led to an enhancement in its capacity to predict settlements.

Without relying on previous monitoring data, the settlement prediction model based on XGBoost could better predict ground settlement through feature simplification. Therefore, this study used the XGBoost algorithm to establish the model and provide an important reference for subsequent engineering applications.

5. Engineering Applications

5.1. Background

The total length of the tunnel project in Nanjing is approximately 1270 m, with a burial depth ranging from 16.4 to 25.5 m. The geological context along the tunnel route is characterized by a high degree of complexity, with the presence of diverse stratigraphic units, including clay, hard rock, and upper soft and lower hard composite strata. The construction parameters are susceptible to significant fluctuations due to the complex geological conditions along the tunnel route, which include a combination of soft and hard strata. These variations in soil composition and depth can impact the efficiency and stability of the construction process. The project profile is illustrated in Figure 12.

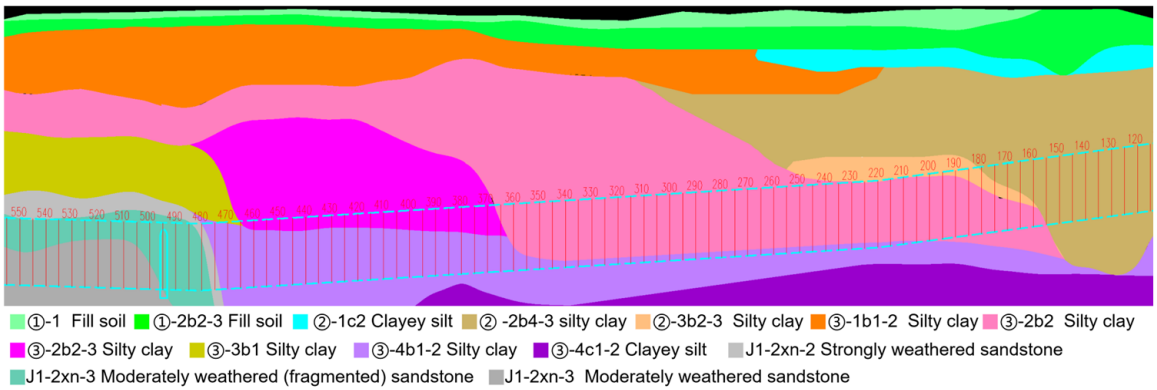

Figure 12. Prediction performance of models under complex geological conditions.

The project was advanced by a soil pressure balance shield machine, and during the construction period, the plan line was variable, including straight lines, gentle curves, and small turning radius sections with a radius of 500 m. Additionally, the elevation line passed through −26.9‰ downhill and 14.2‰ uphill. The geological and construction environment of the project was characterized by a high degree of complexity and variability.

5.2. Experimental Results

5.2.1. Effectiveness

The shield machine proceeded into the airport area at ring 250 and continued until the end of ring 520, for a total length of approximately 324 m. In this area, settlement monitoring was restricted to weekly checks to ascertain the extent of subsidence and uplift. However, the airport stipulated that the shield excavation must be conducted in a manner that would not compromise the integrity of the airport grounds. This presented a significant challenge to the construction process, necessitating a more precise settlement prediction model.

MISPM was applied to this project to predict the change in the ground settlement. This approach allowed us to address the issue of delayed knowledge of settlement, thereby providing valuable support for on-site decision-making.

Before the utilization of the model for the real-time prediction of settlement and the facilitation of decision-making, the data obtained from the initial 200 rings during the construction of the shield machine was employed for training and testing. The training set and test set were divided according to a ratio of 4:1. Following the advancement of each ring, the model employed the construction data from the initial five rings to predict the ground settlement of the current ring and its associated trend. Following the training of the settlement prediction model, the test set was employed to assess its predictive performance. The resulting precision was 0.88, with a recall and accuracy of 0.82.

To ensure the reliability of the model predictions beyond ring 250, the model was used for prediction from ring 200 onwards. The credibility of the predictions for rings 200–250 was then analyzed to confirm whether it could be continued after entering the airport area.

5.2.2. Validation

To verify the accuracy of the settlement prediction model, the engineering team initiated the model validation process at ring 200. At 21:30 on 17 May, following the advancement of ring 221, the model predicted the location of the potential subsidence at the cutter head of the shield machine and issued a medium-grade settlement alarm.

Subsequently, the constructor conducted a comparative analysis of the ground settlement at 16:00 on 17 May, when the shield was advanced to ring 220. The analysis revealed that the settlement was minimal, indicating that no adjustments were necessary to the construction parameters. However, subsequent ground monitoring conducted the following day (at 08:00 on the 18th) revealed a notable increase in ground settlement, as shown in Figure 13.

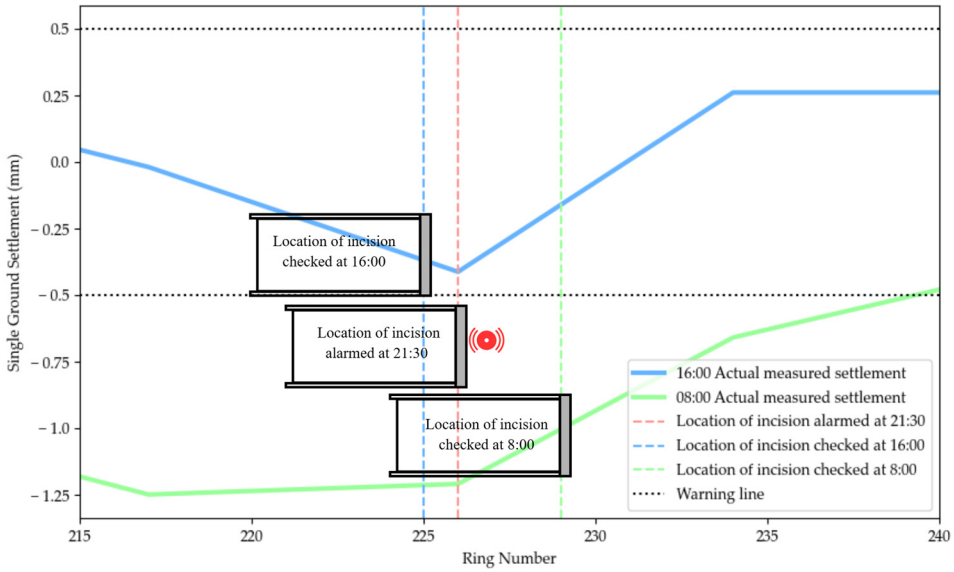

Figure 13. Ground subsidence during the two monitoring periods before and after.

It can be seen that the model was accurate in predicting the ground settlement. It not only coincided with the actual monitoring data but also made the prediction 11 h earlier than the on-site monitoring, verifying the accuracy and timeliness of MISPM in predicting the trend of ground settlement. Following this alarm, the site personnel identified the settlement prediction model presented in this paper. During the subsequent construction phase, they implemented adjustments to the cutting pressure under the model's warnings, thereby ensuring the safety and quality of the shield construction.

5.2.3. Results

The shield machine made its way into the airport area from 23 May onwards, advancing for a total of 36 days. Table 8 illustrates the combined effects of the settlement prediction model and the pressure adjustment in the field, along with the resulting warnings, during this process.

Table 8. Model prediction and pressure adjustment during the airport crossing process.

Time	Ring	Settlement Prediction	Warning Level	On-Site Action
5/26 19:49	276	Subsidence	Medium	Increased from 2.95 bar to 3.0 bar
5/31 21:46	319	Subsidence	Medium	Increased from 3.1 bar to 3.15 bar
6/3 1:33	335	High subsidence	High	Increased from 3.15 bar to 3.25 bar
6/8 17:24	383	Heave	Medium	Reduced from 3.25 bar to 3.20 bar
6/9 7:47	388	Heave	Medium	Reduced from 3.20 bar to 3.15 bar
6/13 15:27	425	High heave	High	Reduced from 3.1 bar to 3.0 bar

Table 8 summarizes the model's predictions and corresponding pressure adjustments during airport transit. For instance, when subsidence was predicted at rings 276 and 319, the warning level was medium, leading to a slight increase in frontal earth pressure by 0.05 bar. Based on the predicted settlement trend and alarm level of the model, this method dynamically adjusts the positive soil pressure to ensure timely and accurate control, demonstrating effectiveness.

5.3. Application Summary

During the weekly on-site inspections at the airport, the concrete pavements were observed to be level and free from deformation or additional cracks. This indicates that the ground settlement remained within a stable range with no significant changes. The settlement prediction model, which integrates mechanics and attitude motion laws, facilitated the construction team's navigation of the airport and was met with considerable acclaim from the engineering community.

MISPM can predict settlement trends quickly and accurately. This can avoid risks from ground movement. Without ground monitoring, the model is also capable of predicting the trend of ground settlement on time, adjusting soil pressure, and ensuring that settlement remains within an acceptable range. The method offers an effective auxiliary decision-making tool for the construction site, facilitating the timely adjustment of construction parameters and proving the method's efficacy and applicability.

6. Conclusions

Based on related theories and research, this paper proposes the mechanism-driven intelligent settlement prediction method (MISPM). According to the relationship between the settlement and the factors of tunnel construction, the ground settlement in front of the shield machine can be accurately predicted. Through simulation and engineering application, results were obtained and verified.

1. This study highlights the supportive role of attitude motion characteristics in settlement prediction and reveals the relationship between various systems during shield construction.
2. By comparing different machine learning algorithms, the use of the XGBoost algorithm combined with reconstruction features improved the prediction accuracy by about 0.1, reaching 0.88. The accuracy and rationality of the model were significantly improved.
3. Compared with actual settlement monitoring, MISPM could also detect settlement changes 11 h in advance, and the accuracy of prediction was 0.82. Without prior monitoring, the method uses the resultant force point and motion center to predict the settlement more quickly and reliably and provides reasonable adjustment suggestions to improve the safety and efficiency of tunnel engineering projects.

Although MISPM has been verified in projects, its generality still needs further verification. Future work can take more parameters into account in the model design to support the adjustment of construction strategies. In addition, this study focuses on predicting

settlement ahead of the tunnel excavation. Tail settlement and cumulative settlement are crucial for environmental safety. It is worth discussing the relationship between the characteristics of the shield tunnel and these two types of settlement trends.

Author Contributions: Conceptualization, M.H. and P.Z.; methodology, M.H., P.Z., J.L. and B.W.; software, P.Z. and B.W.; validation, M.H. and P.Z.; investigation, M.H. and P.Z.; data curation, P.Z. and J.L.; writing—original draft preparation, M.H. and P.Z.; writing—review and editing, M.H. and P.Z.; visualization, P.Z. All authors have read and agreed to the published version of the manuscript.

Funding: This research received no external funding.

Institutional Review Board Statement: Not applicable.

Informed Consent Statement: Not applicable.

Data Availability Statement: The data presented in this study are available on request from the corresponding author. The data are not publicly available due to the specificity of research work.

Conflicts of Interest: All authors declare that the research was conducted in the absence of any commercial or financial relationships that could be construed as a potential conflict of interest.

References

1. Sun, F.; Jin, Z.; Wang, C.; Gou, C.; Li, X.; Liu, C.; Yu, Z. Case Study on Tunnel Settlement Calculations during Construction Considering Shield Disturbance. *KSCE J. Civ. Eng.* **2023**, *27*, 2202–2216. [CrossRef]
2. Cao, L.; Fang, Q.; Zhang, D.; Chen, T. Subway Station Construction Using Combined Shield and Shallow Tunnelling Method: Case Study of Gaojiayuan Station in Beijing. *Tunn. Undergr. Space Technol.* **2018**, *82*, 627–635. [CrossRef]
3. Zhu, C.; Wang, S.; Peng, S.; Song, Y. Surface Settlement in Saturated Loess Stratum during Shield Construction: Numerical Modeling and Sensitivity Analysis. *Tunn. Undergr. Space Technol.* **2022**, *119*, 104205. [CrossRef]
4. Zhang, J.; Xu, M.; Cui, M.; Xin, Y.; Wang, H.; Su, P. Prediction of Ground Subsidence Caused by Shield Tunnel Construction Under Hidden Karst Cave. *Geotech. Geol. Eng.* **2022**, *40*, 3839–3850. [CrossRef]
5. Jin, D.; Yuan, D.; Li, X.; Zheng, H. Analysis of the Settlement of an Existing Tunnel Induced by Shield Tunneling Underneath. *Tunn. Undergr. Space Technol.* **2018**, *81*, 209–220. [CrossRef]
6. Li, K.; Tang, L.; Xie, X.; Zhou, B.; Wen, M. Collaborative Methods for the Ground Settlement Control in Shield Tunnels: Based on Numerical Simulation, GPR Detection and Ground Monitoring. In Proceedings of the 2022 8th International Conference on Hydraulic and Civil Engineering: Deep Space Intelligent Development and Utilization Forum (ICHCE), Xi'an, China, 25–27 November 2022; pp. 244–251.
7. Luo, M.; Wang, D.; Wang, X.; Lu, Z. Analysis of Surface Settlement Induced by Shield Tunnelling: Grey Relational Analysis and Numerical Simulation Study on Critical Construction Parameters. *Sustainability* **2023**, *15*, 14315. [CrossRef]
8. Wang, Z.; Zhang, K.; Wei, G.; Li, B.; Li, Q.; Yao, W. Field Measurement Analysis of the Influence of Double Shield Tunnel Construction on Reinforced Bridge. *Tunn. Undergr. Space Technol.* **2018**, *81*, 252–264. [CrossRef]
9. Chen, R.-P.; Zhang, P.; Kang, X.; Zhong, Z.-Q.; Liu, Y.; Wu, H.-N. Prediction of Maximum Surface Settlement Caused by Earth Pressure Balance (EPB) Shield Tunneling with ANN Methods. *Soils Found.* **2019**, *59*, 284–295. [CrossRef]
10. Bai, X.-D.; Cheng, W.-C.; Li, G. A Comparative Study of Different Machine Learning Algorithms in Predicting EPB Shield Behaviour: A Case Study at the Xi'an Metro, China. *Acta Geotech.* **2021**, *16*, 4061–4080. [CrossRef]
11. Hu, M.; Zhang, B.; Lu, M. Application of BP Neural Network in Prediction of Ground Settlement in Shield Tunneling. In Proceedings of the 2021 IEEE/ACIS 19th International Conference on Computer and Information Science (ICIS), Shanghai, China, 23–25 June 2021; pp. 29–35.
12. Zhou, X.; Zhao, C.; Bian, X. Prediction of Maximum Ground Surface Settlement Induced by Shield Tunneling Using XGBoost Algorithm with Golden-Sine Seagull Optimization. *Comput. Geotech.* **2023**, *154*, 105156. [CrossRef]
13. Zhang, W.-S.; Yuan, Y.; Long, M.; Yao, R.-H.; Jia, L.; Liu, M. Prediction of Surface Settlement around Subway Foundation Pits Based on Spatiotemporal Characteristics and Deep Learning Models. *Comput. Geotech.* **2024**, *168*, 106149. [CrossRef]
14. Ning, X.; An, Y.; Ju, L.; Wang, W. Real-Time Online Prediction of Surface Settlement Considering Spatiotemporal Characteristics during Foundation Excavation. *Autom. Constr.* **2023**, *150*, 104831. [CrossRef]
15. Su, J.; Wang, Y.; Niu, X.; Sha, S.; Yu, J. Prediction of Ground Surface Settlement by Shield Tunneling Using XGBoost and Bayesian Optimization. *Eng. Appl. Artif. Intell.* **2022**, *114*, 105020. [CrossRef]
16. Vu, M.N.; Broere, W.; Bosch, J. Volume Loss in Shallow Tunnelling. *Tunn. Undergr. Space Technol.* **2016**, *59*, 77–90. [CrossRef]

17. Yang, X.; Yang, Z.; Hou, G.; Jiang, Y.; Shao, X.; Qi, W. Evaluation of the Active Limit Support Pressure for Shield Tunnel Face in Clay–Sand Interface Mixed Ground. *Int. J. Geomech.* **2022**, *22*, 04022095. [CrossRef]
18. Zou, J.; Chen, G.; Qian, Z. Tunnel Face Stability in Cohesion-Frictional Soils Considering the Soil Arching Effect by Improved Failure Models. *Comput. Geotech.* **2019**, *106*, 1–17. [CrossRef]
19. Liu, W.; Wan, S.; Fu, M. Limit Support Pressure on Tunnel Face at Different Construction Line Slopes by Slip Line Method. *Tunn. Undergr. Space Technol.* **2020**, *106*, 103619. [CrossRef]
20. Shen, X.; Yuan, D.-J.; Jin, D.-L. Influence of Shield Attitude Change on Shield–Soil Interaction. *Appl. Sci.* **2019**, *9*, 1812. [CrossRef]
21. Chen, H.; Li, X.; Feng, Z.; Wang, L.; Qin, Y.; Skibniewski, M.J.; Chen, Z.-S.; Liu, Y. Shield Attitude Prediction Based on Bayesian-LGBM Machine Learning. *Inf. Sci.* **2023**, *632*, 105–129. [CrossRef]
22. Li, Y.; Bian, X.; Peng, H.; Zhu, B.; Zhou, Y. Additional Stress of Soil and Surface Settlement during Tunnel Shield Construction. *Buildings* **2023**, *13*, 1437. [CrossRef]
23. Wang, G.; Fang, Q.; Du, J.; Wang, J.; Li, Q. Deep Learning-Based Prediction of Steady Surface Settlement Due to Shield Tunnelling. *Autom. Constr.* **2023**, *154*, 105006. [CrossRef]
24. Hu, D.; Hu, Y.; Yi, S.; Liang, X.; Li, Y.; Yang, X. Surface Settlement Prediction of Rectangular Pipe-Jacking Tunnel Based on the Machine-Learning Algorithm. *J. Pipeline Syst. Eng. Pract.* **2024**, *15*, 04023061. [CrossRef]
25. Zhang, W.G.; Li, H.R.; Wu, C.Z.; Li, Y.Q.; Liu, Z.Q.; Liu, H.L. Soft Computing Approach for Prediction of Surface Settlement Induced by Earth Pressure Balance Shield Tunneling. *Undergr. Space* **2021**, *6*, 353–363. [CrossRef]
26. Yang, P.; Yong, W.; Li, C.; Peng, K.; Wei, W.; Qiu, Y.; Zhou, J. Hybrid Random Forest-Based Models for Earth Pressure Balance Tunneling-Induced Ground Settlement Prediction. *Appl. Sci.* **2023**, *13*, 2574. [CrossRef]
27. Ling, X.; Kong, X.; Tang, L.; Zhao, Y.; Tang, W.; Zhang, Y. Predicting Earth Pressure Balance (EPB) Shield Tunneling-Induced Ground Settlement in Compound Strata Using Random Forest. *Transp. Geotech.* **2022**, *35*, 100771. [CrossRef]
28. Zhou, J.; Shi, X.; Du, K.; Qiu, X.; Li, X.; Mitri, H.S. Feasibility of Random-Forest Approach for Prediction of Ground Settlements Induced by the Construction of a Shield-Driven Tunnel. *Int. J. Geomech.* **2017**, *17*, 04016129. [CrossRef]
29. Cheng, Y.; Zhou, W.-H.; Xu, T. Tunneling-Induced Settlement Prediction Using the Hybrid Feature Selection Method for Feature Optimization. *Transp. Geotech.* **2022**, *36*, 100808. [CrossRef]
30. *GB 50911-2013*; Beijing Urban Construction Survey and Design Institute Co. Ltd. Technical Specification for Inspection of Urban Rail Transit Engineering. China Architecture & Building Press: Beijing, China, 2013.
31. Pan, Y.; Qin, J.; Hou, Y.; Chen, J.-J. Two-Stage Support Vector Machine-Enabled Deep Excavation Settlement Prediction Considering Class Imbalance and Multi-Source Uncertainties. *Reliab. Eng. Syst. Saf.* **2024**, *241*, 109578. [CrossRef]
32. Cheng, M.-Y.; Khitam, A.F.K.; Wang, N.-C. Self-Tuning Inference Model for Settlement in Shield Tunneling: A Case Study of the Taipei Mass Rapid Transit System's Songshan Line. *Struct. Control Health Monit.* **2023**, *2023*, 6780235. [CrossRef]
33. Wu, X.; Wang, L.; Chen, B.; Feng, Z.; Qin, Y.; Liu, Q.; Liu, Y. Multi-Objective Optimization of Shield Construction Parameters Based on Random Forests and NSGA-II. *Adv. Eng. Inform.* **2022**, *54*, 101751. [CrossRef]
34. Gu, Z.; Cao, M.; Wang, C.; Yu, N.; Qing, H. Research on Mining Maximum Subsidence Prediction Based on Genetic Algorithm Combined with XGBoost Model. *Sustainability* **2022**, *14*, 10421. [CrossRef]
35. Bo, Y.; Guo, X.; Liu, Q.; Pan, Y.; Zhang, L.; Lu, Y. Prediction of Tunnel Deformation Using PSO Variant Integrated with XGBoost and Its TBM Jamming Application. *Tunn. Undergr. Space Technol.* **2024**, *150*, 105842. [CrossRef]
36. Zhang, N.; Zhou, A.; Pan, Y.; Shen, S.-L. Measurement and Prediction of Tunnelling-Induced Ground Settlement in Karst Region by Using Expanding Deep Learning Method. *Measurement* **2021**, *183*, 109700. [CrossRef]
37. Ye, X.-W.; Ma, S.-Y.; Liu, Z.-X.; Chen, Y.-B.; Lu, C.-R.; Song, Y.-J.; Li, X.-J.; Zhao, L.-A. LSTM-Based Deformation Forecasting for Additional Stress Estimation of Existing Tunnel Structure Induced by Adjacent Shield Tunneling. *Tunn. Undergr. Space Technol.* **2024**, *146*, 105664. [CrossRef]
38. He, Y.; Chen, Q. Construction and Application of LSTM-Based Prediction Model for Tunnel Surrounding Rock Deformation. *Sustainability* **2023**, *15*, 6877. [CrossRef]
39. Ma, J.; Ma, C.; Li, T.; Yan, W.; Faradonbeh, R.S.; Long, H.; Dai, K. Real-Time Classification Model for Tunnel Surrounding Rocks Based on High-Resolution Neural Network and Structure–Optimizer Hyperparameter Optimization. *Comput. Geotech.* **2024**, *168*, 106155. [CrossRef]